The Cryosphere Discuss., https://doi.org/10.5194/tc-2017-189
Manuscript under review for journal The Cryosphere
Discussion started: 18 September 2017

The Cryosphere Discussions
Open Access
EGU

Detecting the permafrost carbon feedback: Talik formation and increased cold-season respiration as precursors to sink-to-source transitions

Nicholas C Parazoo[1], Nicholas.c.parazoo@jpl.nasa.gov

Charles D. Koven[2], cdkoven@lbl.gov

David M. Lawrence[3], dlawren@ucar.edu

Vladimir Romanovsky[4], veromanovsky@alaska.edu

Charles E. Miller[1], Charles.E.Miller@jpl.nasa.gov

[1]Jet Propulsion Laboratory, California Institute of Technology, Pasadena, California, 91109, USA

[2]Lawrence Berkeley National Laboratory, Berkeley, California, USA

[3]National Center for Atmospheric Research, Boulder, Colorado, USA

[4]Geophysical Institute UAF, Fairbanks, Alaska, 99775, USA

The Cryosphere Discuss., https://doi.org/10.5194/tc-2017-189
Manuscript under review for journal The Cryosphere
Discussion started: 18 September 2017

Abstract

Thaw and release of permafrost carbon (C) due to climate change is likely to offset increased vegetation C uptake in Northern High Latitude (NHL) terrestrial ecosystems. Models project that this permafrost C feedback may act as a slow leak, in which case detection and attribution of the feedback may be difficult. The formation of talik, a sub-surface layer of perennially thawed soil, can accelerate permafrost degradation and soil respiration, ultimately shifting the C balance of permafrost affected ecosystems from long-term C sinks to long-term C sources. It is imperative to understand and characterize mechanistic links between talik, permafrost thaw, and respiration of deep soil C to detect and quantify the permafrost C feedback. Here, we use the Community Land Model (CLM) version 4.5, a permafrost and biogeochemistry model, in comparison to long term deep borehole data along North American and Siberian transects, to investigate thaw driven C sources in NHL (> 55°N) from 2000-2300. Widespread talik at depth IS projected across most of the NHL permafrost region (14 million km^2) by 2300, correlated to increased cold season warming, earlier spring thaw, and growing active layers. Talik formation peaks in the 2050s in warm permafrost regions in the sub-Arctic. Comparison to borehole data suggests talik formation may even occur sooner. Accelerated decomposition of deep soil C following talik onset shifts the surface balance of photosynthetic uptake and litter respiration into long-term C sources across 3.2 million km^2 of permafrost. Talik driven sources occur predominantly in warm permafrost, but sink-to-source transition dates are delayed by decades to centuries due to high ecosystem productivity. In contrast, most of the cold permafrost region in the northern Arctic (3 million km^2) shifts to a net source by the end of the 21st century in the absence of talik due to the high decomposition rates of shallow, young C in organic rich soils coupled with low productivity. Our results provide important clues signaling imminent talik onset and C source transition including: (1) late cold season (Jan-Feb) soil warming at depth (~2 m), (2) increasing cold season emissions (Nov-Apr), (3) enhanced respiration of deep, old C in warm permafrost and young, shallow C in organic rich cold permafrost soils. Our results suggest a mosaic of processes that govern carbon source-to-sink transitions at high latitudes, and emphasize the urgency of monitoring soil thermal profiles, organic C age and content, cold season CO_2 emissions, and atmospheric $14CO_2$ as key indicators of the permafrost C feedback.

The Cryosphere Discuss., https://doi.org/10.5194/tc-2017-189
Manuscript under review for journal The Cryosphere
Discussion started: 18 September 2017

1. Introduction

The future trajectory of the Arctic Boreal Zone (ABZ) as a carbon (C) sink or source is of global importance due to vast quantities of C in permafrost and frozen soils (Belshe et al. 2013). Cold and waterlogged conditions in the ABZ have hindered soil organic material (SOM) from microbial decomposition and led to long-term C accumulation at soil depths below 1 m (Ping et al. 2015). Arctic warming, which stimulates plant growth as well as respiration in tundra ecosystems (Euskirchen et al. 2012; Natali et al. 2012; Mack et al. 2004; Barichivich et al. 2013; Commane et al. 2017), has driven a period of C cycle intensification over the last 50 years with greater C inputs and outputs across high latitude ecosystems (Graven et al. 2013). Expert assessments of site-level observations, inversion studies, and process models suggest that Arctic C balance is near neutral, but large uncertainties allow for solutions ranging from small sources to moderate sinks; however, most assessments favor an overall strengthening of the regional C sink, with productivity gains exceeding respiration losses on average (McGuire et al. 2012).

The effect of continued warming on future northern high latitude (NHL) ecosystem C balance is uncertain but appears to be increasingly dependent on responses to changes in cold season emissions, soil moisture, shifts in vegetation community, and permafrost degradation (Abbott et al. 2016). These vulnerabilities are likely driven by disproportionate warming during the cold season (Fraser et al. 2014), which is projected to increase at twice the rate of summer warming over the next century (Christensen et al. 2013). For example, winter warming during the long cold season promotes increased soil respiration, offsetting C uptake during the short Arctic growing season (Oechel et al. 2014; Euskirchen et al. 2016; Commane et al. 2017), and shifting tundra ecosystems from C sink to source (Webb et al. 2016). Winter warming also promotes earlier and more rapid snow melt and landscape thawing (Goulden 1998; Schuur et al. 2015). This can impact seasonal C balance through increased hydrological export of SOM by Arctic rivers (Olefeldt & Roulet 2014), which is projected to increase by 75% by end of century (Abbott et al. 2016). Early snow melt can also cause increased exposure of the land surface to solar absorption (Lawrence et al. 2012) resulting in increased evapotranspiration and summer drought risk (Zhang et al. 2011), which decreases terrestrial biomass through reduced plant growth and increased intensity

and frequency of boreal fire emissions and fire disturbance (Yi et al. 2014; Veravebeke et al., 2017). ABZ fire-driven C losses are expected to increase four-fold by 2100 (Abbott et al. 2016).

On longer time scales, permafrost degradation and resulting C losses from deep, old C is expected to be the dominant factor affecting future Arctic C balance (McGuire et al. 2012; Lawrence et al. 2015; Schuur et al. 2015). In addition to these effects, warmer temperatures and longer non-frozen (NF) seasons caused by earlier spring thaw and later autumn freezing can promote accelerated deepening and increased duration of the active layer (layer of soil near the surface which is unfrozen in summer and frozen in winter) and thawing permafrost. This can initiate formation of a talik zone (perennially thawed sub-surface soils) during active layer adjustment to new thermal regimes (Jorgenson et al. 2010). Talik as well as longer, deeper active layer thaw stimulate respiration of soil C (Romanovsky & Osterkamp 2000; Lawrence et al. 2008), making the ~1000 Pg C in near surface permafrost vulnerable to decomposition (Tamocai et al. 2009; Harden et al. 2012).

Climate models used in the Coupled Model Intercomparison Project Phase 5 (CMIP5) consistently project widespread loss of permafrost in the future due to climate warming [Slater and Lawrence, 2013], though the ESMs that participated in the CMIP5 also project NHL terrestrial C uptake rather than losses due to warming (Ciais et al., 2013). This projection conflicts with expectations from field studies (Schuur et al., 2009; Natali et al., 2014), but newer approaches, such as explicitly representing the vertical structure of soil respiration and its coupling to deep soil thermal changes, lead to changes in the model-projected response from a net C gain with warming to a net loss, and hence a positive carbon-climate feedback (Koven et al. 2011).

Permafrost C emissions are likely to occur gradually over decades to centuries, and therefore are unlikely to cause abrupt and easily detected signals in the global C cycle or climate (Schuur et al. 2015). We use the coupled permafrost and biogeochemistry Community Land Model Version 4.5 (CLM4.5) to investigate in detail the subsurface thermal processes driving C emissions from shallow (0-3m) and deep (>3m) permafrost C stocks and to project the rate of NHL permafrost C feedbacks (> 55°N) over the 21st century. Using CLM4.5 in the framework of an observing system simulation experiment (e.g., Parazoo et al., 2016), we ask how we might be able to (1) identify potential thresholds in soil thaw, (2) detect the specific changes in soil thermal regimes that lead

The Cryosphere Discuss., https://doi.org/10.5194/tc-2017-189
Manuscript under review for journal The Cryosphere
Discussion started: 18 September 2017

104 to changes in ecosystem C balance, and (3) project future C sources following talik onset. We
105 hypothesize that talik formation in permafrost triggers accelerated respiration of deep soil C and,
106 ultimately, NHL ecosystem transition to long-term C sources.

107 Comparison to observed thaw at selected tundra and forested ecosystems along north-south
108 transects in Siberia and North America in the 20th and early 21st century provides a reference to
109 evaluate historical thaw patterns and projected thaw rates. The remainder of our paper is
110 organized as follows: Section 2.1 describes our methods to simulate and analyze soil thaw and C
111 balance in CLM4.5; Section 2.2 describes borehole datasets used to analyze CLM4.5 soil thermal
112 regime; Section 3.1 presents results of talik formation in CLM4.5 and comparison of simulated
113 thaw profiles to borehole data in North America; Section 3.2 evaluates projected thaw rates
114 against long-term borehole data in Siberia; Section 3.3 identifies timing and location of C source
115 onset and discusses formation mechanisms in the presence and absence of talik; Section 3.4
116 presents a projection of future C sources at talik locations; Sections 4 discusses the main findings.

117

118 **2. Methods**

119 *2.1 Simulations*

120 CLM4.5 provides an accurate characterization of the physical and hydrological state of
121 permafrost needed to evaluate permafrost vulnerability and identify key processes (Swenson et
122 al. 2012; Lawrence et al. 2008). CLM4.5 includes a basic set of permafrost processes to allow
123 projection of permafrost carbon–climate feedbacks, including snow schemes, vertically resolved
124 SOM dynamics and soil hydrology, coupled hydraulic and thermal properties in frozen and
125 unfrozen soils allowing realistic seasonal evolution of the active layer, and interaction with
126 shallow (0-3m) and deep (>3m) permafrost C (Swenson et al. 2012; Oleson et al. 2013; Koven et
127 al. 2013, 2015; Lawrence et al. 2008). The soil grid includes 30 vertical levels that has a high-
128 resolution exponential grid in the interval 0–0.5 m and fixed 20-cm layer thickness in the range
129 of 0.5–3.5 m to maintain resolution through the base of the active layer and upper permafrost,
130 and reverts to exponentially increasing layer thickness in the range 3.5–45 m to allow for large
131 thermal inertia at depth.

We use CLM4.5 configured as described in two recent permafrost studies (Lawrence et al. 2015; Koven et al. 2015) using time-varying meteorology, N deposition, CO_2 concentration, and land use change to capture physiological (i.e., CO_2 fertilization) and climate effects of increasing CO_2 over the period 2006-2300. We use an anomaly forcing method to repeatedly force CLM4.5 with observed meteorological from the CRUNCEP dataset for the period 1996–2005 (data available at dods.ipsl.jussieu.fr/igcmg/IGCM/BC/OOL/OL/CRU-NCEP/) and monthly anomalies added based on a single ensemble member from a CCSM4 Representative Concentration Pathway 8.5 (RCP8.5) simulation. The period from 1996 to 2015 represents a base climatological period used for calculating monthly anomalies, with a 20-y record chosen to minimize large anomalies in the first few years. This process is repeated for all variables and all times from 2006 to 2300 (constantly cycling through the same 1996–2005 observed data).

We caution that we are using only a single ensemble member from CCSM4, and hence our results represent one realization from one model forced with one climate scenario. This results in uncertainties from the historical climate/weather forcing, the structure and parameterization of the model, and climate scenarios (both across models and across emissions scenarios).

Simulations are carried out on a global domain at a grid resolution of 1.25° longitude x 0.9375° latitude and saved as monthly averages. Simulation output is collected into decadal averages from 2011-2300 (e.g., 2011-2020 averages for the 2010s, 2021-2030 for the 2020s, etc). Our method to link C balance changes to permafrost thermal state relies on identifying the timing of two key processes: (1) talik formation, and (2) C source transition. Talik formation represents a critical threshold of permafrost thaw. The C source transition represents a shift of ecosystem C balance from a neutral or weak C sink to a long-term source driven by onset of permafrost thaw and respiration of deep SOM (Koven et al. 2015). Using the hypothesis that talik formation triggers a transition to long-term C sources, we quantify the extent of talik formation and rate of transition to C source once talik has formed in permafrost-affected NHL ecosystems.

Following Koven et al. (2015), we define the timing of C source transition from net annual sink to net source as the first decade when annual net biome production (NBP) decreases below -25 g C m^{-2} y^{-1} and remains a source (NBP < 0 g C m^{-2} y^{-1}) through 2300. Here, we use the sign convention of NBP < 0 to represent net C flux from land to atmosphere (e.g., source). The

timing of talik formation is defined as the first decade when soil temperature (T_s) for any layer between 0 and 40 m exceeds -0.5°C for all months in a calendar year (Jan-Dec), assuming that soils start off as permafrost at the beginning of our simulations in 2006. We use a negative freezing point threshold to account for availability of liquid water below 0°C due to freezing point depression. We note the real threshold temperature at which liquid water remains available varies depending on the soil salinity or mineral content, the latter effect of which is included in the actual respiration calculations used by CLM. Here we use -0.5°C as the freeze/thaw cutoff, and examine cutoffs at 0.5°C increments from 0°C to -2.0°C.

We introduce the thawed volume-time integral, or "thaw volume", as a metric to better understand thaw dynamics and help identify thaw instability thresholds. We integrate permafrost in both time (month of year) and depth (soil layer from the surface to 40 m) into a logical function that is one for thawed layers (T_s > -0.5°C), zero for frozen layers, and multiply each thawed layer by layer thickness to convert to units of meter months. This conversion accounts for non-uniform layer thicknesses, providing a consistent metric for comparing simulated and observed thaw.

Our analysis focuses on NHL grid points within the ABZ north of 55°N. We analyze talik formation and C source transitions in the context of the simulated initial state of SOM, and published maps of permafrost conditions from NSIDC (https://nsidc.org/data/docs/fgdc/ggd318_map_circumarctic/) and described in Brown et al. (2001). Permafrost extent is classified as continuous (90-100%), discontinuous (50-90%), sporadic (10-50%).

2.2 Observations

We compare simulated patterns of active layer dynamics and soil thaw to patterns observed from contemporary and historical borehole measurements of permafrost temperature profiles. We focus on sites in western North America and eastern Siberia with daily continuous observations year-round (Jan-Dec) over multiple consecutive years. The primary focus of data in North America (2004-2013) is to evaluate seasonal progression of soil thaw and talik formation near the surface (0-3 m). Siberian data, which have a longer record on average (1950-1994), are

used to evaluate long term trends in soil thaw at 0.0 - 3.6 m depth. Site locations are shown in Fig. 1.

Siberian data are based on measurements along the East Siberian Transect (EST) (https://arcticdata.io/metacat/metacat/doi:10.5065/D6Z036BQ/default). The EST consists of 13 sites that cover a southwest-to-northeast transect in east Siberia [60.7°N, 114.9°E to 68.3°N, 145°E] during the period 1882-1994 (Romanovsky et al. 2007). For this study, we focus on the 9 sites which report measurements as monthly averages at regular depths of 0.2, 0.4, 0.8, 1.6, and 3.2 m. Unfortunately, data gaps of years to decades exist on a site-by-site basis, and many years do not report the full annual cycle over multiple layers. We therefore only analyze years with at least 10 months yr^{-1} of reported monthly mean soil temperature at each layer, and 55 months across the 5 layers (out of 60 possible layer-months per year). Based on these requirements, we find that 6 of 9 sites yield at least 6 years of data over multiple decades, and are well suited for examining historical thaw trends. For comparison to projected trends in CLM4.5, we recalculate observed trends using the inter-site average from all 9 sites at 3 unique locations: northern Siberia (67°N, 144°E), southwest Siberia (61°N, 115°E), and southeast Siberia (59°N, 131°E). Site information is shown in more detail in Table 1.

North American transect data are taken from the global terrestrial network for permafrost (GTNP) borehole database (http://gtnpdatabase.org/boreholes): (1) Borehole 1108 at Mould Bay in Canada [119°W, 76°N] from 2004-2012; (2) Borehole 33 in Barrow along the northern coast of Alaska [156°W, 71.3°N] from 2006-2013; and (3) Borehole 848 in Gakona in southeast Alaska [145°W, 62.39°N] from 2009-2013. Mould Bay is a continuous permafrost tundra site with measurements at 63 depths from 0 - 3 m. Barrow is a continuous permafrost tundra site with measurements at 35 depths from 0 - 15 m. Gakona is a continuous permafrost forest tundra site with measurements at 36 depths from 0 - 30 m. All datasets are reported as daily averages. For each site, we aggregate from daily to monthly averages requiring at least 20 days $month^{-1}$ at each layer and for each year. Measurements are reported at multiple depths and high vertical resolution (up to 0.1 m in shallow layers) but are generally non-uniform in depth (multiple layers missing, different layers reported for each site). Given these inconsistencies

and records <= 8 years, we use these data for qualitative analysis of seasonal and vertical patterns in permafrost thaw. Site information is shown in more detail in Table 2.

3. Results

3.1 Simulated Talik Onset in the 21st Century

Our simulations show widespread talik formation throughout Siberia and northern North America over the period 2010-2300 (Fig. 1A), impacting ~14.5 million km^2 of land in NHL's (55°-80°N) assuming a freeze/thaw threshold of -0.5°C. 10.6 million km^2 of land in Europe, southwest Asia, and N. America (below 60°N) either formed talik prior to the start of our simulation in 2010 in regions already experiencing degraded permafrost (e.g., Fig. 1D, permafrost extent < 90% in southwest Siberia and southern N. America), or did not have permafrost to begin with. A small amount of land along northern coastal regions (~1.6 million km^2) show no talik formation prior to 2200.

The long-term trend and decadal variability of talik formation are quantitatively and qualitatively similar for freeze/thaw thresholds at or below -0.5°C (Fig. 1B). Peak formation generally occurs over the period 2050-2150, accelerating rapidly early in the 21st century, and leveling off in the late 22nd century. The timing and location of talik formation correlates with the annual mean temperature of permafrost at 3 m ($T_{soil\text{-}3m}$) (Fig. 1C) and observed permafrost state (Fig. 1D, from Brown et al. 2001) at the start of our simulation; we see earlier talik formations in sub-Arctic regions (< 66N) with warm simulated permafrost ($T_{soil\text{-}3m}$ > 0°C) and permafrost extent less than 90%, and later formation in northern regions with cold permafrost ($T_{soil\text{-}3m}$ < 0°C) and continuous permafrost. Talik formation progresses northward from the sub-Arctic to the Arctic over time, starting in the warm/discontinuous permafrost zone in the 21st century then to the cold/continuous permafrost zone the 22nd century. This suggests a shift in permafrost state across the pan-Arctic from continuous to discontinuous over the next 2 centuries.

Our simulations demonstrate consistent patterns of changing thaw volume leading up to and following initial talik formation, independent of the decade of talik onset. Time series of thaw volume as a function of decade relative to talik onset (Fig. 2A) show a steady rise in thaw

245 volume of 1-2 m months yr^{-1} in the decades prior to talik formation, with thaw limited primarily
246 to shallow soils (< 1.5 m) and summer/early fall. Thaw volume accelerates to 10-20 m months
247 yr^{-1} within 1-4 decades of talik onset, coinciding with thaw penetration at depth (~2 meters on
248 average, Fig. 2B) and deeper into the cold season (~Jan-Apr). Thaw penetration into the Jan-Apr
249 period occurs for the first time at 2.6 ± 0.9 decades prior to talik onset (vertical grey lines in Fig.
250 2A). At talik onset, thaw volume jumps from mean values of 60 ± 10.7 m months yr^{-1} to 377 ±
251 44 m months yr^{-1} at a mean depth of 4.1 meters. Thaw volume levels out within one decade
252 following initial talik formation and accelerated thaw of all soil layers; this leveling is an artifact
253 of the maximum depth of soils in CLM4.5 (equal to 45.1 meters), and represents the complete
254 transition from permafrost to seasonally-frozen ground in the model. The transition to deep
255 cold season thaw and rapidly increasing thaw volume represent key threshold signaling
256 imminent talik onset.

257 Onset of surface thaw in the uppermost soils during the spring freeze/thaw transition provides
258 another reliable predictor for talik onset. In particular, we find consistent dates and trends of
259 spring thaw in the surface soil layer in the decades leading up to talik onset (Fig. 2C), shifting by
260 about 1 week over 4 decades from Day of Year (DOY) 134 ± 2.8 (~mid May) to DOY 127 ± 3.5
261 during talik formation (~early May).

262 Changes in total column soil water and sub-surface drainage following talik onset may provide
263 clues a posteriori that talik is already present. Lawrence et al. (2015) show that deepening of
264 the active layer and thawing of permafrost allows water to drain deeper into the soil column,
265 which dries out near surface soils. Our simulations show a similar drying pattern in shallow
266 layers (~0-1 m depth) in the 4 decades prior to talik onset (Fig. 2D). This does not significantly
267 impact total water storage as it is primarily a redistribution of water within the column;
268 however, there are significant changes in water balance following talik onset, including rapid
269 increase in sub-surface drainage and decrease in volumetric soil moisture, as discussed below.

270 The time evolution of soil vertical thermal and hydrological structure for the subset of grid cells
271 that form talik in the 2090s is shown in more detail in Fig. 3. Here, we have subtracted the
272 thermal and hydrological profiles in the 2040s to show relative change. The 4 decades prior to
273 talik onset are shown in Fig. 3A-D (2050s – 2080s), the decade of talik onset in Fig. 3E (2090s),

and the 4 decades following talik onset in Fig. 3F-I (2100s – 2130s). CLM4.5 represents the process of soil thawing as passage of a "thaw front" in space and time through soil layers, penetrating and warming colder, deeper layers, and bringing the frozen soil environment at depth closer to thermodynamic equilibrium with the warming atmosphere. At 4 decades prior to talik onset (Fig. 3A), our simulated thawed layer exhibits a tilted time-depth profile with earlier thaw and longer thaw duration (~4-5 months) in the near surface (< 1 m) compared to later thaw and reduced thaw duration (1-2 months) at maximum thaw depth (~ 2 m). In the 3 decades leading up to talik onset, we find more pronounced tilting of the thawed layer with time and depth, with gradual deepening to 3-4 m and penetration of thaw period into Jan-Feb.

Our simulations indicate an increased rate of heat transfer and thawing at depth following talik onset, leading to rapid subsequent thawing, drying, and decrease in the thickness of the seasonally frozen layer above talik (Fig. 3 E-I). This rapid thawing is depicted in Fig 2A as the large jump in thaw volume, and in Fig. 2D as enhanced drying and drainage, with drying peaking at 3.5-4.5 m depth. In our simulations, talik onset effectively pulls the "bath plug" that was the ice filled pore space at depth, with year round ice-free conditions allowing soil water to percolate and be diverted to sub-surface drainage (Lawrence et al., 2015). We note that bedrock soil is not hydrologically active in CLM4.5, and thus the rate of thawing and drainage in response to permafrost thaw may be underestimated in deeper CLM4.5 layers near bedrock due to reduced heat capacity.

Our simulated pattern of phase lag for heat transfer to depth mimics observed thaw profiles in N. America (Fig. 4), which are sensitive to latitude and ecosystem, but with more "vertical" time-depth tilt in CLM4.5 compared to observations. Borehole data shows shallow (~0.5 m) and seasonally short (~3-4 months from Jun-Sep) thaw at the northernmost tundra site in the Canadian Archipelago (Fig. 4A; 76°N, Mould Bay), shallow but longer thaw (5 months from Jun-Oct) moving slightly south to North Slope Alaska (Fig. 4B; 71.3°N, Barrow), and deep (~3 m) and seasonally long (May-Feb) thaw at the low latitude continental boreal site in southeast Alaska (Fig. 4C; 62.4°N, Gakona). CLM4.5 shows reduced depth and seasonal duration of thaw when sampled at these specific geographical points, although the north-south gradient of increasing thaw moving south is preserved (Fig. 4D-F). Given the challenging task of comparing point

303 locations with grid cell means, we also examine the mean behavior of CLM4.5 at locations
304 where soil temperature at depth is similar to that observed. Accounting for permafrost
305 temperature at 3 meters (by sampling all locations with $T_{soil\text{-}3m}$ within 0.5°C of the observed
306 temperature) better reproduces thaw depth, but with reduced seasonal duration throughout
307 the soil column (Fig. 4G-I). These results suggest the current ensemble CLM4.5 run
308 overestimates the rate of soil refreeze in early fall.

309 Based on the pattern of January and February thaw/freeze dynamics observed at Gakona in the
310 2010s and the time lag of 1-3 decades from this occurrence to talik onset in our simulations, we
311 project that Gakona will form talik as early as the 2020s, assuming the atmosphere continues to
312 warm as prescribed in CLM4.5. Talik onset in CLM4.5 is variable in this region with earliest onset
313 by mid-century (~2050s, Fig. 1A); however, our comparison to observations suggests that
314 simulated thaw rates in this region and for similar permafrost temperatures are
315 underestimated, and that earliest onset may occur sooner than predicted. Overall, we find that
316 simulated patterns of permafrost thermal state change are consistent with available
317 observations, but that the exact thaw rates are uncertain. We keep these uncertainties in mind
318 as we examine patterns of change and talik formation simulated into 2300.

319 *3.2 Evaluation of Simulated Thaw Rates and Talik Onset Against Siberian Borehole Data*

320 The Siberian borehole locations have similar permafrost extent (> 50%) to the North American
321 locations according to the Circumpolar Permafrost Map (Brown, 2001) and similar mean annual
322 air temperature (~ -13.6°C) in the 2000s according to CLM4.5. However, air temperature is
323 more seasonal in Siberia, including colder winters (4°C colder) and warmer summers (6°C
324 warmer). Spring thaw for the Siberian sites occurs two weeks earlier on average than for the
325 North American sites in the 2000s, but follows the same pattern of later thaw date moving
326 north along the borehole transect.

327 Next we examine thaw trends observed from borehole soil temperature data in Siberia in the
328 20th century and evaluate patterns of CLM4.5 projected trends in the 21st century. We note
329 several caveats in these comparisons: (1) model simulations are based on only one realization
330 (i.e., model ensemble member) of historic and future warming and projected permafrost thaw,

(2) availability and access of long term records in Siberia is limited, and (3) there is significant variability in space and time in simulated and observed thaw rates, making direct comparisons challenging. These comparisons thus serve primarily as a first benchmark for future model analysis and development.

We focus first on site-specific long-term trends by analyzing the 5 Siberian borehole sites which recorded at least 5 years of data spanning multiple decades: Drughina, Lensk, Macha, Uchur, and Chaingda. Records at these locations show a decrease in thaw volume with an average of 0.19 m months yr^{-1} from 1955 – 1990 (Table 1, Fig 5). All sites except Drughina show negative trends, with larger trends in southern locations, ranging from 0.51 m months yr^{-1} from 1957-1990 at Chaingda in southern Siberia, to a statistically insignificant trend of -0.083 months yr^{-1} from 1969-1990 at Drughina in northeastern Siberia, suggesting a more or less constant thermal state at this site. Further examination indicates that active layer thickness at Drughina actually decreased to 0.8 meters from 1989-1990 compared to 1.2 meters in the 1970s. Drughina also shows smaller average thaw volume magnitude compared to other sites, consistent with shallower thaw (layer thickness increases exponentially with depth along the Siberian transect). Together, these findings indicate that active layer thickness is decreasing at Drughina.

The average trend at 3 long term stations in southwest Siberia clustered at [60.7°N, 114.9°E] is -0.18 m months yr^{-1}, which is a factor of 3 weaker compared to Chaingda station (thaw rate = 0.51 m months yr^{-1}; $p < 0.05$) slightly south and 15° to the east (59.0°N 130.6°E). Each of these permafrost sites exhibits talik at various times between 1957 and 1990 (vertical dashed line), with earlier talik onset to the west (1957 at Lensk, 1970 at Macha, 1974 at Uchur) and later talik onset to the east (1989 at Chaingda). The presence of talik reflects an increase in the depth and duration of thaw late into the cold season, rather than a physical decrease in soil thaw as appears to be the case at Drughina. We acknowledge the difficulty in identifying talik onset due to discontinuities in the dataset and limited vertical information; however, we note that the 15-30 year gap between talik formation in the western site cluster vs Chaingda 15° east is geographically consistent with model simulations of later talik formation in eastern Siberia in the 21st century (Fig. 1A) and thus may represent a gradual expansion of warming into the east.

In general, permafrost appears to be degrading more rapidly at the southern locations compared to the northern location.

We recompute observed thaw trends at regional clusters using combined records at the 2 sites in northern Siberia, 6 sites in southwest Siberia, and 1 site in southeast Siberia (Table 1) and compare these to thaw projections in CLM4.5 (Fig. 6). The simulated trend in thaw volume shows a change in sign at northern locations (blue), acceleration of thaw at southwest sites (orange), and reduction of thaw at the southeast sites (brown). Despite the change in sign in northern Siberia representing a possible shift from net permafrost accretion to net thaw in the mid 21st century, thaw projections indicate continued stability of permafrost through the early 22st century. Our simulations show a shift to accelerated soil thaw beginning in the early 2080s, marked by onset of deep soil thaw late in the cold season (January, denoted by cyan circle).

Thaw projections in the southern locations show more abrupt shifts in the magnitude of thaw volume in the 21st century. Projected thaw volume is generally on track with borehole data at the western locations, but deviate strongly from the single record at Chaingda. Despite observed talik onset as early as the 1970s in the southwest (Macha and Uchar) and late 1980s in the southeast (Chaingda), simulated talik onset is not projected to occur until the 2030s at the western sites (orange) and the 2080s at the eastern sites (brown). The strong discrepancy between observed and simulated thaw and talik onset in southern Siberia warrants close monitoring and continued investigation of this region through sustained borehole measurements and additional model realizations of potential future warming.

3.3 Carbon Cycle Responses to Changing Ground Thermal Regime

Fig. 7A plots the decade in which NHL ecosystems are projected to transition to long-term C sources over the next 3 centuries (2010-2300). A total of 6.8 million km^2 of land is projected to transition, peaking in the late 21st century, with most regions transitioning prior to 2150 (4.8 million km^2 or 70%, Fig. 7B, solid black). At first, pan-Arctic C fluxes remain neutral on average over the early- to mid- 21st century (2010-2070) as increasing productivity and C sinks dominate large scale C balance (Fig. 7B, purple). The spatially integrated pan-Arctic C balance increasingly favors net C source dominance over the next 100 years, peaking at 0.7-0.8 Pg C in the mid- to

late- 22nd century, followed by gradual decline to 0.5 Pg C by 2300. The cumulative C source over the entire simulated period (2010-2300) is 11.6 Pg C.

Most regions (6.2 million km^2 of land, or 91%) identified as a C source also form talik at some time during the simulation (Fig. 7C). However, the geographic pattern of C sink-to-source transition date is reversed compared to that of talik formation, with earlier transitions at higher latitudes (the processes driving these patterns are discussed in detail below). Overall, the lag relationship between talik onset and C source transition exhibits a tri-modal distribution (Fig. 7D), with peaks at negative time lag (C source leads talik onset, Median Lag = -5 to -6 decades), neutral time lag (C source synchronized with talik onset; Median Lag = -2 to 1 decade), and positive time lag (C source lags talik; Median Lag = 12 decades; red shading in Fig. 7C). Roughly half of these regions (3.2 million km^2) show neutral or positive time lag (lag ≥ 0). This pattern, characteristic of the sub-Arctic (< 65°N), represents the vast majority of C source transitions after 2150 (Fig. 7B, dotted). The remaining regions (3.0 million km^2) in the Arctic and high Arctic (> 65°N) show negative time lag and account for most of late 21st century sources (Fig. 7B, dashed). C sources in the regions not identified as talik (0.63 million km^2) either show talik presence at the start of our simulation, or are projected to transition in the absence of permafrost or in regions of severely degraded permafrost (Fig. 7C, dash dotted).

Here, we investigate biological and soil thermal processes driving these relationships, focusing first on regions where C source transition leads talik onset (blue shading in Fig. 7C). In these, thaw volume is low (< 50 m months yr^{-1}) and shows a weak relationship to NBP (NBP increases much faster than thaw volume) prior to C source onset (indicated by large green circle in Fig. 8A). By the time thaw volume reaches 300 m months yr^{-1} and talik formation occurs, these regions are already very strong sources (NBP > 150 g C m^{-2} yr^{-1}). This suggests that C sources in these regions are not driven by respiration of old C from deep soil thaw, and thus alternative explanations are needed.

Closer examination of thermal and moisture dynamics in shallow soils reveals three potential indicators of C source transition: (1) seasonal duration of thaw, (2) depth of thaw, and (3) soil drying. For example, vertical profiles of soil temperature and moisture (Fig. 9) in regions which transition to C sources in the 2090s show deeper seasonal penetration of soil thaw, a jump in

417 active layer growth, and enhanced year round soil drying during the C source transition decade
418 (Fig. 9D). A broader analysis of soil thaw statistics over all regions and periods indicates that C
419 source transitions are most common when active layers grow to 1-2 meter depth and thaw
420 duration penetrates to Oct or Nov for the first time (Fig. 10).

421 Further examination of ecosystem biogeochemistry also shows high initial C stocks in these
422 regions (red shading in Fig. 7E). The median initial state of soil organic matter (SOM), 109 kg C
423 m^{-2}, is nearly a factor of 2 larger than the median value in regions where C source lags talik
424 onset (SOM = 59 kg C m^{-2}). These regions also show 40% less gross primary production (median
425 GPP = 755 vs 1296 g C m^{-2} yr^{-1}) and higher over saturation prior to C source onset (water filled
426 pore space at 0.5 m depth at 10, 5, and 2 decades prior = 0.63, 0.59, and 0.57 mm3 mm^{-3} for
427 cold permafrost, vs a near constant value of 0.57 mm3 mm^{-3} in warm permafrost). The total
428 area of land in which SOM exceeds 100 kg C m^{-2} represents 2/3 of all land where C sources lead
429 talik onset (2.0 million km^2), and peaks at a negative time lag of -5 to -6 decades (Fig. 7D, green
430 bars), which perfectly aligns with the peak distribution of negative time lags. These results
431 indicate peat like conditions characterized by saturated soils, high C stocks, and low annual
432 productivity which allow low thaw volumes (active layer depth < 2 m and peak thaw month of
433 October, on average) and rapid soil drying to produce early C losses in colder environments in
434 the absence of talik.

435 In regions where C source transitions lag talik onset (red shading in Fig. 7C), NBP is strongly
436 sensitive to changes in thaw volume until C source onset occurs (Fig. 8B), and talik formation
437 occurs when these regions are weak sinks (NBP < 0 g C m^{-2} yr^{-1}). In general, C sources in these
438 regions are more sensitive to C emissions from deep soil thaw. However, as noted above,
439 neutral and positive time lags show a bimodal distribution peaking near 0 and 15 decades, and
440 thus additional explanations are needed. Further examination shows high fire activity in these
441 regions at the time of C source onset (red shading in Fig. 7F). The regions where fire C emissions
442 exceed 25 g C m^{-2} yr^{-1}, representing our threshold for C source transition, are exclusively boreal
443 ecosystems, account for 1/3 of all land with negative lags (~1.1 million km^2), and align perfectly
444 with the peak distribution of positive time lags (Fig. 7D, red bars). NBP is less sensitive to thaw
445 volume in regions where fire dominates the C balance, which are strong C sinks at talik onset

(Fig. 8C), where soil C respiration is 13% less than non-fire regions (median SOM-HR = 331 vs 382 g C m^{-2} yr^{-1}), and productivity is 25% more (median GPP = 1548 vs 1216 g C m^{-2} yr^{-1}). Fire regions are also 28% drier on average in the surface layer than non fire regions (volumetric soil moisture = 0.28 vs 0.39 mm3 mm-3 in summer (May-Sep) in the upper 10 cm of soil). These results suggest that soil thermal processes and talik formation are significant factors driving C source transition in regions with reduced productivity, but fire activity, spurred by soil drying, drives C source transition in higher productivity regions.

Figure 11 presents histograms of total permafrost area (Fig. 11A) and mean GPP (Fig. 11B) as a function of decades since talik onset. We removed regions with high initial soil organic matter (SOM > 100 kg m^{-2}, green bars in Fig. 7D) and fire C emissions (Fire > 25 g C m^{-2} yr^{-1}, red bars in Fig. 7D) during the C source transition decade. This screening yields a more normal distribution of the decadal time lags between talik onset and C source transition (Fig. 11A), with a mean lag of 1 decade form talik onset to C source. The high standard deviation of lags (± 8 decades) reflects the skewed distribution of GPP (Fig. 11B); very low productivity in cold permafrost increases the likelihood that soil thaw will lead to C source transition, while very high productivity in warm permafrost decreases this likelihood.

Independent of the presence of talik, a key effect of an increasing number of thaw months is an increasing rate of respiration from soil C pools. Warming and CO_2 fertilization increase the rate of photosynthetic C uptake, increasing soil respiration mainly from younger near-surface C pools; whereas deeper thawing affects both young and old C pools, so that the depth of thaw dictates the timing and dominant C age of the net respiration flux. Fig. 12 illustrates this with a comparison of decadal respiration trends for SOM (SOMHR) and litter (LITHR) C pools for C source transitions in the mid 21st century, for scenarios where C source leads talik onset (blue line, cold permafrost) and lags talik (red lines, warm permafrost). Here, we examine total respiration (SOMHR+LITHR) and respiration difference (SOMHR=LITHR) from soil and litter C pools.

GPP and total respiration show nearly linear increases (~15% per decade) for each permafrost regime surrounding the decade of C source transition with peak fluxes in the growing season (Fig. 12 A - D). Total respiration in cold permafrost is systematically larger than in warm

permafrost in the growing season (May – Sep) and smaller in the cold season (Oct – Apr). In particular, total respiration is effectively zero for the late cold season (Jan – Apr) in cold permafrost and significantly positive in warm permafrost over the same period. The respiration difference also increases surrounding the C source transition (Fig. 12 E - F), but with 2 key differences from total respiration: (1) the decadal increase is exponential, starting from a value near zero just 3 decades prior to C source transition, and (2) peak respiration difference occurs in late summer / early fall. Because litter respiration in the model is mainly drawing from C pools with short turnover times, the litter respiration flux equilibrates rapidly to changes in productivity and thus its change primarily reflects changes to inputs rather than decomposition rates. Conversely, soil C pools, which have much longer turnover times, equilibrate much more slowly to the productivity changes and thus primarily reflect changes to the turnover times. The trend in soil vs litter respiration explains almost the entire trend in net ecosystem C balance from neutral to net source (Fig. 12 G – H). Furthermore, warm permafrost shows sustained dominance of soil respiration during the entire cold season. These results are consistent with an increasing thaw effect on C budgets during C source transitions, but where shallow thaw of young soil C dominates in cold permafrost, and where talik formation and deep thaw of old soil C dominate warm permafrost.

These results suggest that where talik forms, soil respiration increases throughout the year as talik and perennial thaw mobilize deeper old soil C to respiration. In the absence of talik in colder environments, soil respiration increases primarily in the NF season due to increased availability of thawed shallow soil C. The lower GPP in colder regions suggests that increased availability of substrate for respiration due to plant growth and soil C accumulation has less impact on C source transition in our simulations than soil thaw dynamics and the initial state of soil C. Thus, cold permafrost locations become C sources due only to thaw-season dynamics while warmer permafrost locations transition to C sources due largely to changes in cold season dynamics.

4 Discussion

503 Talik formation is widespread in our simulations, affecting ~14.5 million km^2 of NHL land in the
504 21st century. Simulations of the vertical thermal structure of soil thaw leading to talik in CLM4.5
505 qualitatively reproduce deep soil temperature data from borehole measurements in Siberia and
506 western North America, although rates of thaw at these and similar permafrost locations are
507 underestimated. Space-for-time comparisons along the north-south borehole transect in Alaska
508 and the Canadian Archipelago show a pattern of deepening and seasonal expansion of thaw
509 moving from the coldest location of the transect in northern Canada (Mould Bay) to the
510 warmest location in southeast Alaska (Gakona). Gakona shows the characteristic late cold
511 season thaw penetration into February at 2-3 meters depth which in our simulations signals
512 imminent talik onset (in the case of Gakona, as soon as the 2020s). Likewise, projected soil
513 thaw trends in east Siberia are in line with long term borehole measurements along the East
514 Siberian Transect, but the rate of talik formation here is also underestimated.

515 These comparisons indicate stable permafrost conditions in the colder sites in Siberia and N.
516 America through the 21st century, where thaw is generally slow, seasonally short, and stable.
517 This suggests talik formation in the northern Arctic is decades to centuries away, but potentially
518 sooner than the early 22nd century as projected by the CLM4.5 simulation. Our analysis finds
519 more unstable permafrost conditions to the south, with observed talik in the late 20th century
520 although simulated talik is delayed until the early 21st century.

521 Due to the potential for early 21st century talik and discrepancy between observed and
522 simulated trends in warm permafrost, continued model investigation of factors controlling the
523 rate of soil thaw is critically needed. In particular, large scale drying as projected in CLM4.5 near
524 the surface (Lawrence et al., 2015) may be restricting heat penetration and active layer growth
525 in the growing season, especially in organic rich soils which have very low thermal conductivity
526 (O'Donnell et al., 2009; Lawrence et al., 2011; 2012). Experiments demonstrating the sensitivity
527 of talik to soil drying within the active layer across soil hydrology schemes in previous (CLM4),
528 current (CLM4.5), and newly available (CLM5) versions of CLM could provide key insight on soil
529 thermal dynamics in frozen or partially frozen conditions.

530 Our simulations show robustly a pattern of accelerated soil C respiration following talik onset,
531 which shifts the surface C balance of photosynthetic uptake and litter respiration from net C

532 sinks to long term net sources across 3.2 million km^2 of NHL land by 2300. The pattern of C
533 source transition following talik formation is most evident in warm permafrost in the sub-Arctic,
534 suggesting increased microbial decomposition with warming soils. We also find evidence of talik
535 driven soil drying near the surface associated with increased active layer thickness and higher
536 available water storage, which can lead to enhanced decomposition rates by causing soils to be
537 less frequently saturated/anoxic (Lawrence et al., 2015). At the same time, these regions show
538 high ecosystem productivity which increases roughly in proportion to respiration, and thus
539 appears to be driven by combination of warming and increased nitrogen availability resulting
540 from permafrost thaw (Mack et al., 2004; Natali et al., 2012; Koven et al., 2015). As such, the
541 transition time to sustained net ecosystem C source is delayed by 1-2 centuries following talik
542 onset as productivity continues to outpace respiration as currently observed (Belshe et al.,
543 2013; Mack et al., 2004), with C balance transitions peaking in the mid- to late 22nd century. In
544 nearly 1/3 of these regions, an estimated 2 million km^2 of land, fires are a primary mechanism
545 triggering C source onset, rather than talik. Consequently, in regions of very high productivity,
546 talik appears to serve more as an indirect driver of long term C sources through accelerated soil
547 drying, rather than as a direct driver through accelerated respiration of deep soil C.

548 We identify an equally large region of land in the high Arctic, representing ~3.0 million km^2,
549 which is projected to transition to long term C sources much sooner than the sub-Arctic and in
550 the absence of talik. This region, distributed across northern Siberia and North America,
551 resembles peatlands and is characterized by cold permafrost, high soil C stocks and soil
552 moisture, and low productivity. Thawing in this cold northern permafrost is limited to young,
553 shallow soils with significantly reduced contributions from deeper, older C than warm
554 permafrost, but with a factor of 2 higher C stocks. These C rich soils become increasingly
555 vulnerable to decomposition as they are exposed to increased warming and drying as active
556 layers deepen and persist deeper into the cold season. The transition to long term C sources in
557 this region peak is expected to peak between 2050 and 2100, nearly a century prior to talik
558 driven sources in warm permafrost, and decades to centuries prior to talik onset, which
559 eventually amplifies C sources in this region.

These results have important implications for designing an Arctic monitoring system to simultaneously detect changes in the soil thermal state and C state. In particular, C observations should not be limited to warm permafrost regions of the sub-Arctic, since cold northern permafrost regions are projected to become C sources even without forming talik. Our analysis of the seasonal dynamics and vertical structure of permafrost thaw and soil C emissions provides a general strategy for concurrent observing warm and cold permafrost based on time of year and depth of thaw.

Observing warm permafrost will require year round measurements of ground thermal state to detect precursors to talik onset including thaw penetration at depth (~2-3 m) and late into the cold season (~Jan-Feb), as well as sustained cold season C flux observations to detect changes in C balance associated decomposition and respiration of deep, old soil C. Continued monitoring of these depths will require sustained long term measurements from deep boreholes, and increasing reliance on remote sensing technologies such as Electromagnetic Imaging (EMI). In particular, EMI surveys along the continuous/discontinuous permafrost transition zones during the cold season from November – March are likely to provide key thermal state diagnostics. Systematic radiocarbon (^{14}C) measurements, which can be used to partition respiration into autotrophic and heterotrophic young and old soil components (Hicks Pries et al. 2015), would provide a valuable tool to help disentangle and track future C emissions from deep permafrost, especially during the long cold season when talik enables the microbial decomposition of deep old C and is the primary source of C emissions.

Observing cold permafrost in the high Arctic is both more urgent, due to earlier shifts in C balance, and more complicated, due to challenging observing conditions (remote, cold, and dark) and less detectable signals in thermal state (e.g., talik) and C age (e.g., depleted in radiocarbon) change. Our results suggest sustained observation of year round soil thermal and hydrological profiles (soil drying; depth and duration of thaw at 1-2 meter depth) using boreholes and EMI surveys, and cold season net CO_2 exchange (Sep – Oct) using atmospheric CO_2 sensors and eddy covariance towers, can help detect changes in soil thaw and soil vs litter respiration driving annual C balance changes. We also recommend an observing network

588 focused on regions rich in soil organic matter, where our simulations indicate increased
589 sensitivity of soil decomposition to warming.

590

591 **5 Conclusion**

592 Greening trends driven by high latitude warming and CO_2 fertilization have led to amplification
593 of the contemporary C cycle, characterized by increasing photosynthetic C uptake during the
594 short growing season and increasing respiration of recent labile soil C during the cold season
595 (Mack et al., 2004; Piao et al., 2008; Randerson et al., 1999; Graven et al., 2013; Forkel et al.,
596 2016; Wenzel et al., 2016; Webb et al., 2016). Our simulations of C-climate feedbacks with
597 interactive terrestrial biogeochemistry and soil thaw dynamics indicate this trend continues
598 mostly unabated in NHL ecosystems. However, sustained warming over the next 300 years
599 drives accelerated permafrost degradation and soil respiration, leading to widespread shifts in
600 the C balance of Arctic ecosystems toward long term net C source by the end of the 23rd
601 century. 6.8 million km^2 of land impacted in Siberia and North America will produce an
602 integrated C source of 11.6 Pg C from 2010-2300, peaking at 0.7-0.8 Pg C yr^{-1} in the mid- to late-
603 22nd century. Our projected permafrost C feedback is comparable to the contemporary land
604 use/land use change contribution to the annual C cycle.

605 Our main results emphasize an emergence of cold season processes driven by amplified winter
606 warming, earlier spring thaw, longer NF seasons, and increased depth and seasonal duration of
607 soil thaw. Our simulations are consistent with soil thaw patterns observed from borehole time
608 series in Siberian and North American transects during the late 20th and early 21st centuries.
609 Patterns of deeper and longer thaw drive widespread talik, and exposes Arctic soils to increased
610 warming and drying, which accelerates decomposition and respiration of deep, old C, and shifts
611 ecosystem C balance to a state increasingly dominated by soil respiration.

612 The timing with which Arctic ecosystems transition to long term net C sources depends on a
613 number of factors including talik onset, vegetation productivity, permafrost temperature, soil
614 drying, and organic matter. The timing is most sensitive to talik onset in warm permafrost
615 regions in the sub-Arctic, which account for a total of 3.2 million km^2 of land, representing ~50%

of our simulated permafrost region. These regions are also the most productive, which can delay the transition to net C source by decades or even centuries. As such, warm permafrost regions typically do not transition to net C sources until the mid-22nd century.

The cold permafrost region in the northern Arctic, which accounts for an additional 3.0 million km^2 of land, transitions to net C source in the late 21st century, much earlier than warm permafrost and in the absence of talik. High decomposition rates, driven by warming and drying of shallow, young C in organic rich soils, and low annual productivity make this region perhaps the most vulnerable to C release and subject to further amplification with future talik onset. This result is surprising given the region is dominated by tundra and underlain by deep, cold permafrost that might be thought impervious to such changes.

Rather than thinking of the permafrost feedback as being primarily driven by a single coherent geographic front driven by talik formation along the retreating boundary of the permafrost zone, this analysis suggests multiple modes of permafrost thaw with a mosaic of processes acting in different locations. Active-layer deepening leads to C sink-to-source transitions in some regions, talik-driven permafrost loss in others, fire-driven changes in other places, and thaw-led hydrologic change in yet others. Our results reveal a complex interplay of amplified contemporary and old C cycling that will require detailed monitoring of soil thermal properties (cold season thaw depth, talik formation), soil organic matter content, soil C age profiles, systematic CO_2 flux, and atmospheric $^{14}CO_2$ measurements to detect and attribute future C sources. Further investigation of soil thermal properties and thaw patterns is required to understand C balance shifts and potential further amplification of emissions from high northern latitudes.

Acknowledgements

DML is supported by U.S. Department of Energy, Office of Biological and Environmental Research grant DE-FC03-97ER62402/A0101. CDK is supported by the Director, Office of Science, Office of Biological and Environmental Research of the US Department of Energy (DOE) under Contract DE-AC02-05CH11231 as part of their Regional and Global Climate Modeling (BGC-

644 Feedbacks SFA), and Terrestrial Ecosystem Science Programs (NGEE-Arctic), and used resources
645 of the National Energy Research Scientific Computing Center, also supported by the Office of
646 Science of the US Department of Energy, under Contract DE-AC02-05CH11231. National Center
647 for Atmospheric Research (NCAR) is sponsored by the National Science Foundation (NSF). The
648 CESM project is supported by the NSF and the Office of Science (BER) of the US Department of
649 Energy. Computing resources were provided by the Climate Simulation Laboratory at NCAR's
650 Computational and Information Systems Laboratory, sponsored by NSF and other agencies.
651 Some of the research described in this paper was performed for CARVE, an Earth Ventures (EV-
652 1) investigation, under contract with NASA. A portion of this research was carried out at JPL,
653 California Institute of Technology, under contract with NASA.

654 **References**

655 Abbott, B.W. et al., 2016. Biomass offsets little or none of permafrost carbon release from soils,
656 streams, and wildfire: an expert assessment. *Environmental Research Letters*, 11(3),
657 p.34014. Available at: http://dx.doi.org/10.1088/1748-9326/11/3/034014.
658 Barichivich, J. et al., 2013. Large-scale variations in the vegetation growing season and annual
659 cycle of atmospheric CO2 at high northern latitudes from 1950 to 2011. *Global Change*
660 *Biology*, 19(10), pp.3167–3183.
661 Belshe, E.F., Schuur, E.A.G. & Bolker, B.M., 2013. Tundra ecosystems observed to be CO2
662 sources due to differential amplification of the carbon cycle. *Ecology Letters*, 16(10),
663 pp.1307–1315.
664 Brown, J. et al., 2001. Circum-Arctic map of permafrost and ground-ice conditions, National
665 Snow and Ice Data Center/World Data Center for Glaciology, Boulder, CO. *Digital Media,*
666 *available at: http://nsidc. org*.
667 Ciais, P., et al., 2013: Carbon and Other Biogeochemical Cycles. In: *Climate Change 2013: The*
668 *Physical Science Basis. Contribution of Working Group I to the Fifth Assessment Report of*
669 *the Intergovernmental Panel on Climate Change* [Stocker, T.F., D. Qin, G.-K. Plattner, M.
670 Tignor, S.K. Allen, J. Boschung, A. Nauels, Y. Xia, V. Bex and P.M. Midgley (eds.)].
671 Cambridge University Press, Cambridge, United Kingdom and New York, NY, USA, pp. 465–
672 570, doi:10.1017/CBO9781107415324.015.
673 Christensen, J.H. et al., 2013. Climate Phenomena and their Relevance for Future Regional
674 Climate Change Supplementary Material. *Climate Change 2013: The Physical Science Basis.*
675 *Contribution of Working Group I to the Fifth Assessment Report of the Intergovernmental*
676 *Panel on Climate Change*, p.62. Available at: www.climatechange2013.org.
677 Commane, R. et al., 2017. Carbon dioxide sources from Alaska driven by increasing early winter
678 respiration from Arctic tundra, Proceedings of the National Academy of Sciences, 114 (21),
679 5361-5366.
680 Euskirchen, E.S. et al., 2012. Seasonal patterns of carbon dioxide and water fluxes in three

representative tundra ecosystems in northern Alaska. *Ecosphere*, 3(1), p.art4.

Euskirchen, E.S, M.S. Bret-Harte, G.R. Shaver, C.W. Edgar, and V.E. Romanovsky, 2016. Long-term release of carbon dioxide from arctic tundra ecosystems in Alaska, *Ecosystems*, DOI 10.1007/s10021-016-0085-9.

Forkel, M., et al., 2016. Enhanced seasonal CO2 exchange caused by amplified plant productivity in northern ecosystems, Science, 351(6274), 696-699.

Fraser, R.H. et al., 2014. Warming-Induced Shrub Expansion and Lichen Decline in the Western Canadian Arctic. *Ecosystems*, 17(7), pp.1151–1168. Available at: http://dx.doi.org/10.1007/s10021-014-9783-3.

Goulden, M.L., 1998. Sensitivity of Boreal Forest Carbon Balance to Soil Thaw. *Science*, 279(5348), pp.214–217.

Graven, H.D. et al., 2013. Enhanced seasonal exchange of CO2 by northern ecosystems since 1960. *Science (New York, N.Y.)*, 341(September), pp.1085–9. Available at: http://www.ncbi.nlm.nih.gov/pubmed/23929948.

Harden, J.W. et al., 2012. Field information links permafrost carbon to physical vulnerabilities of thawing. *Geophysical Research Letters*, 39(15), pp.1–6.

Hicks Pries, C.E. et al., 2015. Decadal warming causes a consistent and persistent shift from heterotrophic to autotrophic respiration in contrasting permafrost ecosystems. *Global Change Biology*, 21(12), pp.4508–4519.

Jorgenson, M.T.T. et al., 2010. Resilience and vulnerability of permafrost to climate changeThis article is one of a selection of papers from The Dynamics of Change in Alaska's Boreal Forests: Resilience and Vulnerability in Response to Climate Warming. *Canadian Journal of Forest Research*, 40(7), pp.1219–1236. Available at: http://dx.doi.org/10.1139/X10-060.

Koven, C.D. et al., 2011. Permafrost carbon-climate feedbacks accelerate global warming. *Proceedings of the National Academy of Sciences of the United States of America*, 108(36), pp.14769–74.

Koven, C.D., Riley, W.J. & Stern, A., 2013. Analysis of permafrost thermal dynamics and response to climate change in the CMIP5 earth system models. *Journal of Climate*, 26(6), pp.1877–1900.

Koven, C.D., Lawrence, D.M. & Riley, W.J., 2015. Permafrost carbon-climate feedback is sensitive to deep soil carbon decomposability but not deep soil nitrogen dynamics. *Proceedings of the National Academy of Sciences of the United States of America*, 112(12), pp.3752–7. Available at: http://www.pnas.org/content/112/12/3752.full.

Lawrence, D.M. et al., 2008. Sensitivity of a model projection of near-surface permafrost degradation to soil column depth and representation of soil organic matter. *Journal of Geophysical Research: Earth Surface*, 113(2).

Lawrence, D.M. et al., 2011. Parameterization improvements and functional and structural advances in Version 4 of the Community Land Model, J. Adv. Model. Earth Syst., 3, Art. 2011MS000045, 27 pp.

Lawrence, D.M., Slater, A.G. & Swenson, S.C., 2012. Simulation of present-day and future permafrost and seasonally frozen ground conditions in CCSM4. *Journal of Climate*, 25(7), pp.2207–2225.

Lawrence, D.M. et al., 2015. Permafrost thaw and resulting soil moisture changes regulate projected high-latitude CO 2 and CH 4 emissions. *Environmental Research Letters*, 10(9),

p.94011. Available at: http://stacks.iop.org/1748-9326/10/i=9/a=094011?key=crossref.0ec3ff97879a814d0c3dfaacde810d23.

Mack, M.C. et al., 2004. Ecosystem carbon storage in arctic tundra reduced by long-term nutrient fertilization. *Nature*, 431(September), pp.440–3. Available at: http://www.ncbi.nlm.nih.gov/pubmed/15386009.

McGuire, A.D. et al., 2012. An assessment of the carbon balance of Arctic tundra: Comparisons among observations, process models, and atmospheric inversions. *Biogeosciences*, 9(8), pp.3185–3204.

Natali, S.M., Schuur, E.A.G. & Rubin, R.L., 2012. Increased plant productivity in Alaskan tundra as a result of experimental warming of soil and permafrost. *Journal of Ecology*, 100(2), pp.488–498.

Natali et al. 2014. Permafrost degradation stimulates carbon loss from experimentally warmed tundra, Ecology, 95(3), 602-608.

O'Donnell, J. A., Romanovsky, V. E., Harden, J. W., McGuire, A. D., 2009. The effect of moisture content on the thermal conductivity of moss and organic soil horizons from black spruce ecosystems in interior Alaska. Soil Science, 174(12), 646-651.

Oechel, W.C. et al., 2014. Annual patterns and budget of CO2 flux in an Arctic tussock tundra ecosystem. *Journal of Geophysical Research: Biogeosciences*, 119(3), pp.323–339.

Olefeldt, D. & Roulet, N.T., 2014. Permafrost conditions in peatlands regulate magnitude, timing, and chemical composition of catchment dissolved organic carbon export. *Global change biology*, 20(10), pp.3122–3136.

Oleson, K.W. et al., 2013. NCAR/TN-503+STR NCAR Technical Note, (July).

Parazoo, N. C. et al. 2016. Detecting patterns of changing CO_2 flux in Alaska, Proc Natl Acad Sci, 113, 28, 7733-7738

Piao S, et al., 2008. Net carbon dioxide losses of northern ecosystems in response to autumn warming. Nature 451(7174), 49–52.

Ping, C.L. et al., 2015. Permafrost soils and carbon cycling. *Soil*, 1(1), pp.147–171. Available at: http://www.soil-journal.net/1/147/2015/.

Randerson, J.R., Field, C. B., Fung, I. Y., Tans, P. P., 1999. Increases in early season ecosystem uptake explain recent changes in the seasonal cycle of atmospheric CO_2 at high northern latitudes, Geophys. Res. Lett., 26(17), 2765-2768.

Romanovsky, V.E. & Osterkamp, T.E., 2000. Effects of unfrozen water on heat and mass transport processes in the active layer and permafrost. *Permafrost and Periglacial Processes*, 11(3), pp.219–239.

Romanovsky, V. E., Sazonova, T. S., Balobaev, V. T., Shender, N. I., and D. O. Sergueev, 2007. Past and recent changes in permafrost and air temperatures in Eastern Siberia, *Global and Planetary Change*, 56: 399-413.

Schuur, E.A.G. et al., 2009. The effect of permafrost thaw on old carbon release and net carbon exchange from tundra. *Nature*, 459(7246), pp.556–559.

Schuur, E.A.G. et al., 2015. Climate change and the permafrost carbon feedback. *Nature*, 520(January 2016), pp.171–179.

Slater, A.G. and Lawrence, D. M., 2013. Diagnosing present and future permafrost from climate models, J. Climate, 26, 5608-5623.

Swenson, S.C., Lawrence, D.M. & Lee, H., 2012. Improved simulation of the terrestrial

hydrological cycle in permafrost regions by the Community Land Model. *Journal of Advances in Modeling Earth Systems*, 4(8).

Tamocai, C. et al., 2009. Soil organic carbon pools in the northern circumpolar permafrost region. *Global Biogeochemical Cycles*, 23(2), pp.1–11.

Veraverbeke, S. et al., 2017. Lightning as a major driver of recent large fire years in North American boreal forests. Nature Climate Change, DOI:10.1038/NCLIMATE3329.

Webb, E.E. et al., 2016. Increased wintertime CO2 loss as a result of sustained tundra warming. J. Geophys. Res. Biogeosci., 121, doi:10.1002/2014JG002795.

Wenzel, S., Cox, P.M., Eyring, V., Friedlingstein, P., 2016. Projected land photosynthesis constrained by changes in the seasonal cycle of atmospheric CO2. Nature, 538, 449-501.

Yi, S. et al., 2014. Freeze/thaw processes in complex permafrost landscapes of northern Siberia simulated using the TEM ecosystem model: Impact of thermokarst ponds and lakes. *Geoscientific Model Development*, 7(4), pp.1671–1689.

Zhang, K. et al., 2011. Changing freeze-thaw seasons in northern high latitudes and associated influences on evapotranspiration. *Hydrological Processes*, 25(26), pp.4142–4151.

The Cryosphere Discuss., https://doi.org/10.5194/tc-2017-189
Manuscript under review for journal The Cryosphere
Discussion started: 18 September 2017

785 **Tables**

786 **Table 1**: Site information for long-term borehole temperature measurements along the East
787 Siberian Transect for the period 1957-1990. The 9 sites reported in this table, presented in a
788 north-to-south order, meet the criteria of at least one year of valid soil temperature data (>= 10
789 months per layer, ≥ 55 months across 5 layers). Talik is observed in 4 of 9 sites, 2 of which is
790 observed in the first year of valid reported data. Site-specific thaw trends are provided for sites
791 with at least 6 years of valid data. Regional trends are calculated from all available data for 3
792 regional locations.

Site	Location	Date Range	Years with Valid Data	First Obs Talik	Site Trend (m mo yr^{-1})	Region	Regional Trend (m mo yr^{-1})
Drughina	145.0°E, 68.3°N	1969-1990	8	N/A	-0.083	N Siberia	-0.057
Ustmoma	143.1°E, 66.3°N	1973-1975	3	N/A	N/A		
Chumpuruck	114.9°E, 60.7°N	1981-1984	4	N/A	N/A	SW Siberia	0.019
Lensk	114.9°E, 60.7°N	1957-1990	11	1957	0.23		
Macha	114.9°E, 60.7°N	1970-1990	13	1970	0.070		
Oimyakon	114.9°E, 60.7°N	1966-1974	6	N/A	0.059		
Tongulakh	114.9°E, 60.7°N	1966-1966	1	N/A	N/A		
Uchur	114.9°E, 60.7°N	1966-1990	17	1974	0.24		
Chaingda	130.6°E, 59.0°N	1967-1990	8	1989	0.51	SE Siberia	0.51

793

794

The Cryosphere Discuss., https://doi.org/10.5194/tc-2017-189
Manuscript under review for journal The Cryosphere
Discussion started: 18 September 2017

795 **Table 2**: Site information for borehole temperature measurements at 3 sites along a north-to-
796 south transect in North America for the period 2004-2012. Climatological soil thermal state
797 presented on a site-to-site basis Fig. 5 are based on all available valid monthly data for each
798 site, with valid data requiring at least 20 days of reported data for each layer. Layer of Deepest
799 Thaw represents the deepest layer in which mean soil temperature exceeds freezing (> -0.5°C)
800 in at least 1 month. Month of Latest Thaw represents the latest month in which mean soil
801 temperature exceeds freezing. Here, we define May as the earliest possible month and April as
802 the latest possible month.

Site	Location	Date Range	Depth / Number of Layers	Layer of Deepest Thaw	Month of Latest Thaw
Mould Bay, Canada	119.0°W, 76.0°N	2004-2012	3 m / 36	0.69 m	September
Barrow2, Alaska	156.0°W, 71.3°N	2006-2013	15 m / 63	0.58 m	October
Gakona1, Alaska	145.0°W, 62.4°N	2009-2013	30 m / 35	2.5 m	February

803

804

The Cryosphere Discuss., https://doi.org/10.5194/tc-2017-189
Manuscript under review for journal The Cryosphere
Discussion started: 18 September 2017

805 **Figures**

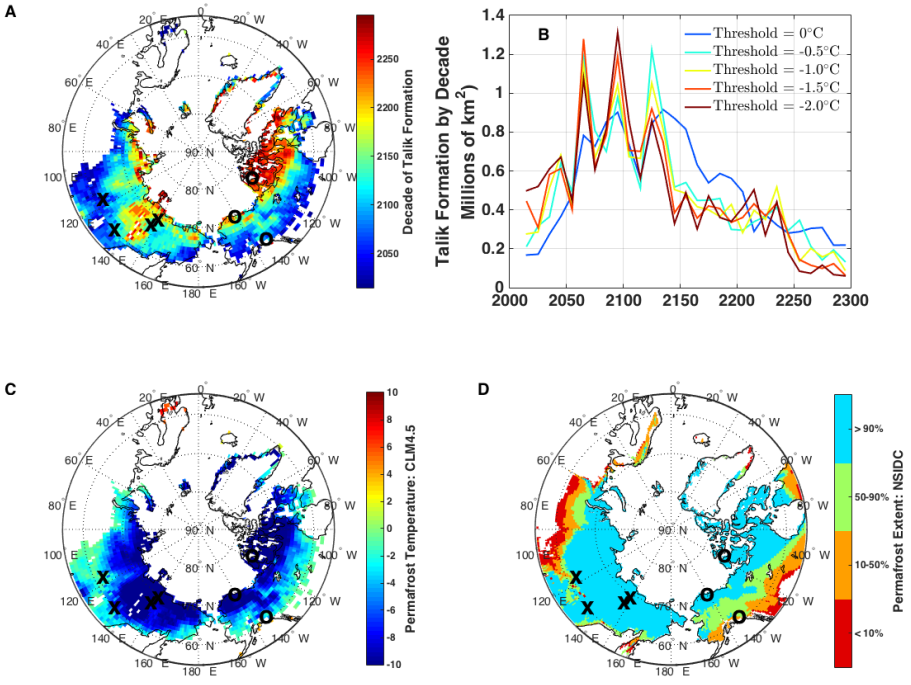

806

807 **Figure 1**. Decade of projected talik formation and correlation to initial state of simulated
808 permafrost temperature and observed permafrost extent. (A) Maps and (B) time series of the
809 simulated decade of talik formation are estimated from CLM4.5 as the first decade when the
810 mean temperature of a soil layer exceeds a freeze/thaw threshold of -0.5°C in every month. (C)
811 Initial permafrost temperature is defined as the annual mean soil temperature at 3 m depth
812 from 2006-2010. (D) Permafrost extent is taken from
813 (https://nsidc.org/data/docs/fgdc/ggd318_map_circumarctic/; Brown et al., 2001). Crosses in
814 A, C, D represent locations of Siberian borehole measurements along the East Siberian Transect
815 from 1955-1900 (Table 1). Circles represent locations of borehole measurements in Alaska and
816 Canada from 2002-2013 (Table 2). We note that peak transition time occurs around 2100.

817

The Cryosphere Discuss., https://doi.org/10.5194/tc-2017-189
Manuscript under review for journal The Cryosphere
Discussion started: 18 September 2017

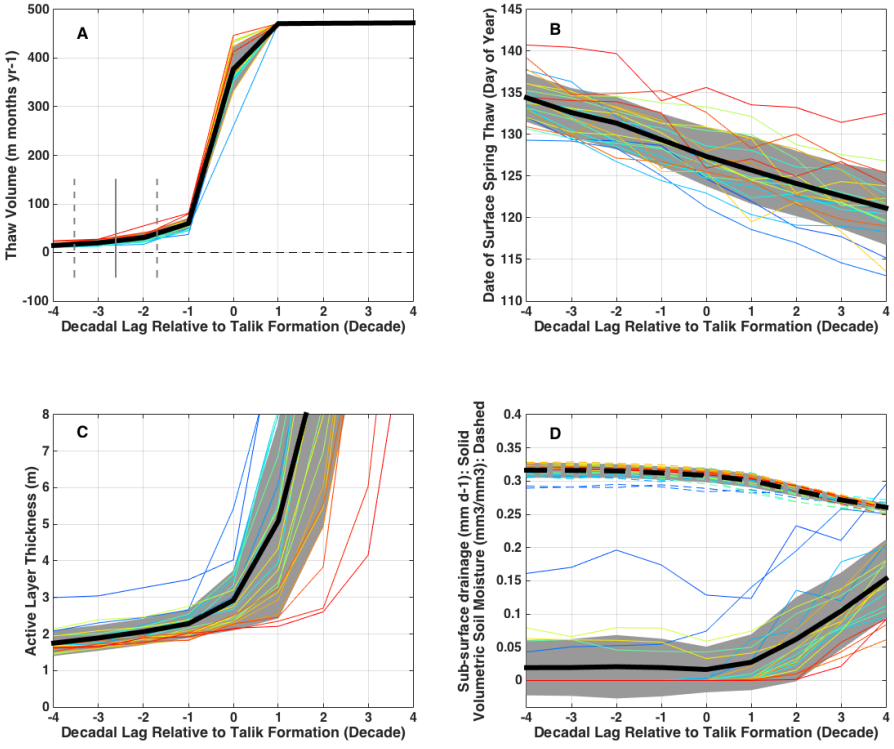

Figure 2. Patterns showing the progression of soil thaw in the decades surrounding talik onset. Individual lines represent averages across the subset of talik forming regions for each decade from the 2050s (darkest red) to the 2250s (darkest blue). (A) Integrated soil thaw volume, where the vertical solid line represents the mean timing of initial thaw at depth and late into the cold season (Jan-Apr). Note that the upper limit to the thaw volume metric in (A) is an artifact of the arbitrary maximum soil depth of 45.1m in CLM4.5. Other panels show (B) Date of spring surface thaw in the uppermost layer, (C) annual maximum active layer thickness, and (D) annual sub-surface drainage (solid) and volumetric soil moisture averaged over the soil column (dashed) and. Grey shaded areas show the standard deviation of results for individual talik formation decades. Mean behavior exhibits a characteristic pattern: gradual increase in thaw volume and active layer depth prior to talik onset, abrupt shift in thaw volume, active layer depth, followed by stabilization to constant thaw volume as soil drying and sub-surface drainage increases.

The Cryosphere Discuss., https://doi.org/10.5194/tc-2017-189
Manuscript under review for journal The Cryosphere
Discussion started: 18 September 2017

833

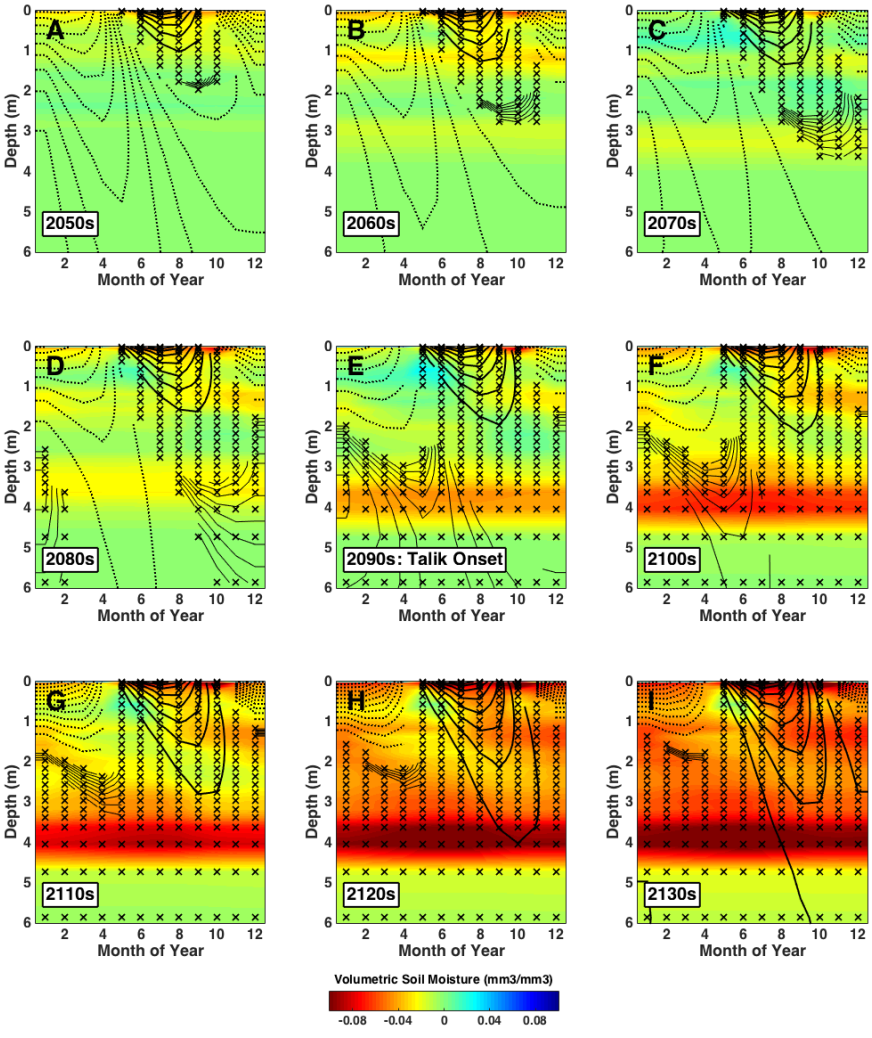

834

835 **Figure 3**. Evolution of simulated decadal thermal and hydrological state as functions of month
836 and depth averaged across talik forming regions in the 2090s. Each panel presents decadal
837 average seasonal profiles in the decades surrounding talik onset from the 2050s (A) to the
838 2130s (I). Contours are soil temperature in 0.5°C intervals, with solid (dashed) lines denoting
839 temperature above (below) a freeze/thaw threshold of -0.5°C. Stars indicate "thaw" months
840 where soil temperature exceeds -0.5°C. Color shading is volumetric soil moisture anomalies
841 relative to the 2040s, where red indicates drying. Note that soil depth on y-axis is plotted on a

842 non-linear scale. The soil thaw profile exhibits a shift from predominantly frozen and wet to
843 perpetually thawed and drying conditions at depth while remaining seasonally frozen near the
844 surface.

845

The Cryosphere Discuss., https://doi.org/10.5194/tc-2017-189
Manuscript under review for journal The Cryosphere
Discussion started: 18 September 2017

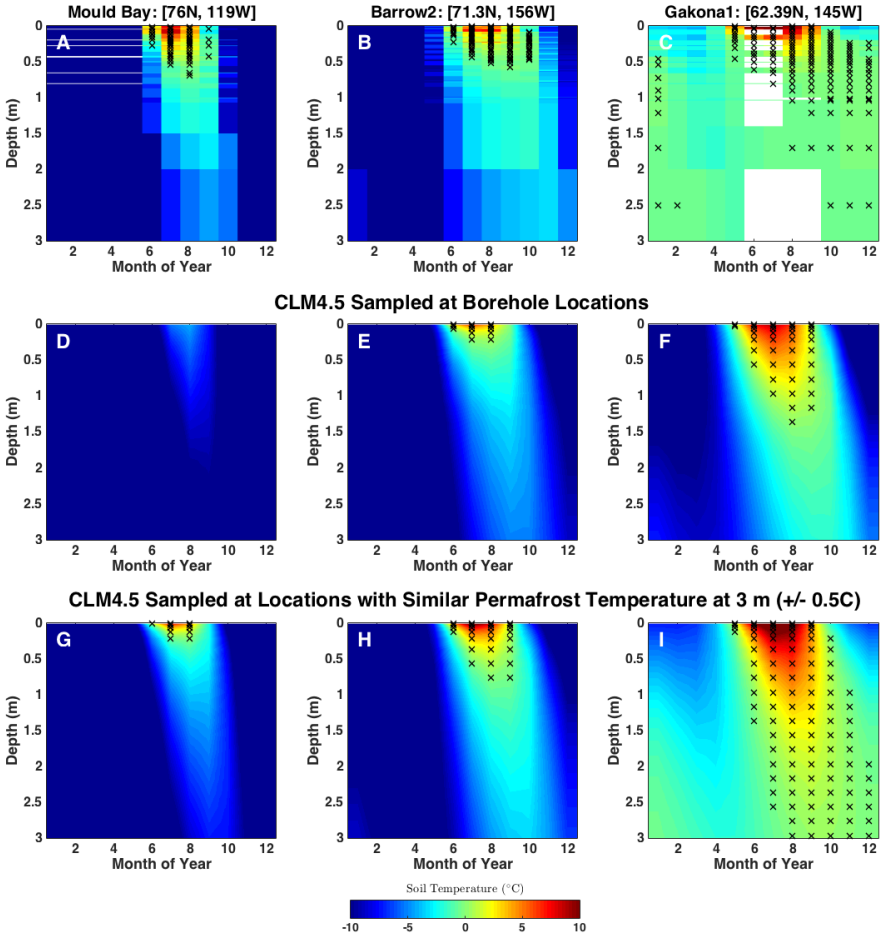

Figure 4. Observed and simulated early 21st century soil thermal state as a function of month and depth for the North American Transect boreholes (black circles, Fig. 1). Top Row: Observed multi-year means for Mould Bay, Canada (2004-2012), Barrow, Alaska (2006-2013), and Gakona, Alaska (2009-2013). The color scale shows the mean temperature and the stars mark the months when each layer is thawed (T > -0.5°C). Simulated soil thermal state from 2006-2010 for borehole locations (Middle Row) and regions with 3 m permafrost temperature within 0.5°C of observed (Bottom Row) show similar north-to-south spatial gradient to observations, especially for similar permafrost temperature. Note that the thaw state at Gakona, Alaska persists at depths of 1-3 m into the deep cold season (Jan-Feb), perhaps signaling the threshold for rapid talik formation (see Fig. 3D).

The Cryosphere Discuss., https://doi.org/10.5194/tc-2017-189
Manuscript under review for journal The Cryosphere
Discussion started: 18 September 2017

857

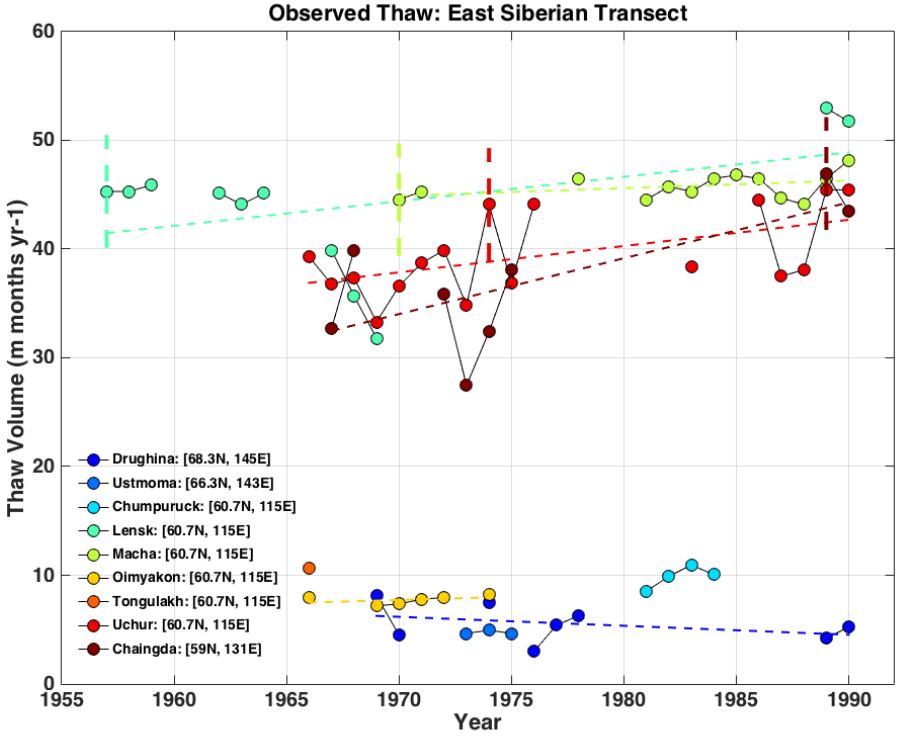

858

859 **Figure 5**. Soil thaw observation time series from borehole measurements of soil temperature at
860 sites along the East Siberian Transect over various periods from 1957 – 1990. Site coordinates
861 are provided in the legend and plotted as crosses on the map provided in Fig. 1. Thaw trends
862 are derived from estimates of thawed volume over a depth of 3.2 m for sites with > 5 years of
863 data over multiple decades: Drughina, Lensk, Macha, Uchur, and Chaingda. Trend values are
864 reported in Table 1. Vertical dashed lines mark the onset of talik formation at Lensk (1957),
865 Macha (1970), Uchur (1974), and Chaingda (1989). Sites in southern Siberia show significant
866 negative thaw volume trends over the 20th century, representing net increases in soil thaw. The
867 trend at Drughina is not statistically significant, indicating that soil thaw is unchanged in
868 northern Siberia.

869

The Cryosphere Discuss., https://doi.org/10.5194/tc-2017-189
Manuscript under review for journal The Cryosphere
Discussion started: 18 September 2017

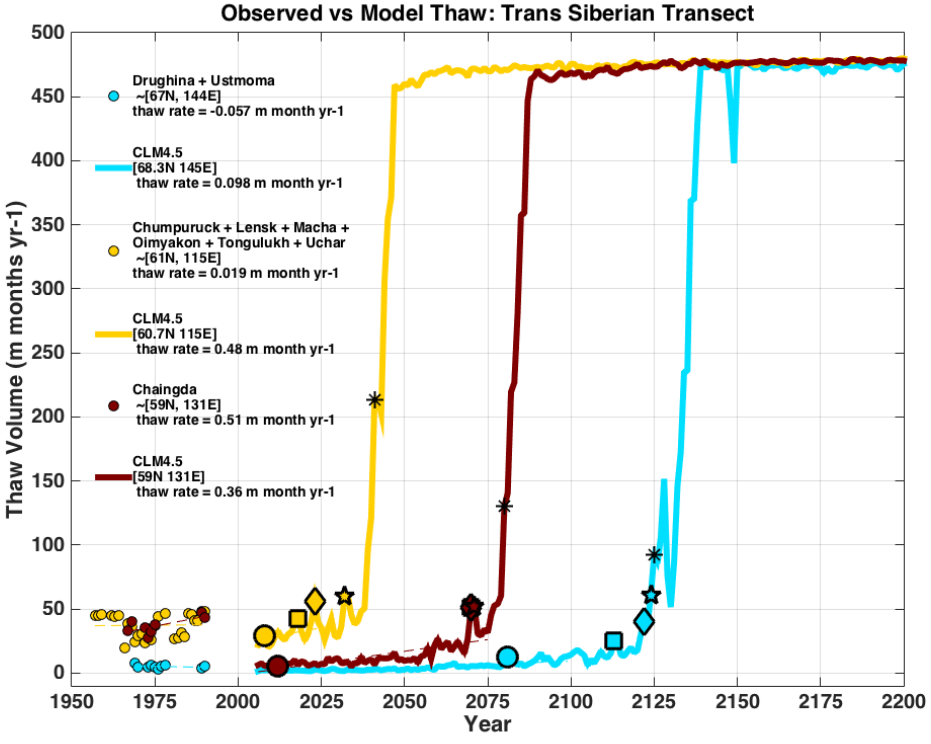

Figure 6. Comparison of 20th century observed (markers) and 21st century projected (solid lines) soil thaw at sites along the East Siberian Transect (crosses in Fig. 1). Observed thaw from 1955-1990 is based on soil thaw data in Fig. 5 and on the inter-site average at 3 locations: northern Siberia (blue), southwest Siberia (orange), and southeast Siberia (brown). Simulated thaw from 2006-2200 is derived from CLM4.5 and sampled at the nearest grid cell of 3 above locations. Markers represent thresholds for thaw onset in January (circle), February (square), March (diamond), April (star), and talik onset (asterisk). Thaw trends are derived from estimates of soil thaw volume. We note a key discrepancy between observed and simulated thaw volume: Simulated thaw volume is integrated over depths from 0-40 meters; observed thaw volume is integrated from 0-3.6 meters. The effect of this selection bias is a potential low bias in observed thaw volume. In general, soil thaw is projected to remain stable in northern Siberia but become increasingly unstable in southern Siberia.

The Cryosphere Discuss., https://doi.org/10.5194/tc-2017-189
Manuscript under review for journal The Cryosphere
Discussion started: 18 September 2017

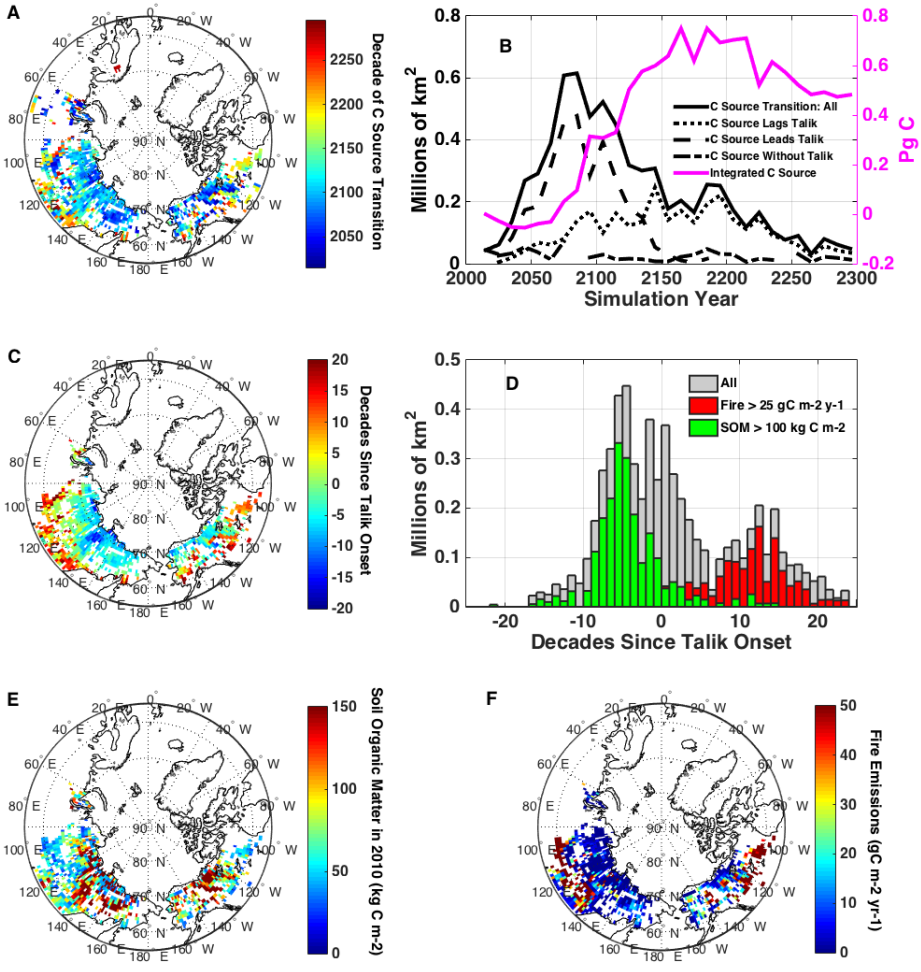

884

885 **Figure 7**. Projected decade when permafrost regions shift to long-term C sources over the
886 period 2010-2300, and relation to talik onset, soil C, and fire emissions. (A) Map of the decade
887 of transition to C source, reflected in the color code, showing earlier transitions in cold northern
888 permafrost. (B) The area of land that transitions peaks in the late 21st century, and is driven by
889 regions where the C source leads talik onset (dashed). The integrated C source from these
890 regions (magenta) peaks in the late 22nd century. (C) The decadal time lag from talik onset to C
891 source transition shows positive lags in warm southern permafrost (C source lags talik) and
892 negative lags in cold norther permafrost (C source leads talik). (D) Histogram shows trimodal

The Cryosphere Discuss., https://doi.org/10.5194/tc-2017-189
Manuscript under review for journal The Cryosphere
Discussion started: 18 September 2017

893 distribution of permafrost area as a function of decadal time lag, with negative lags related to
894 high soil organic matter (green bars and map in E), and large positive lags related to fires (red
895 bars and map in F) but delayed by high productivity (Fig. 11B). See text for details.

896

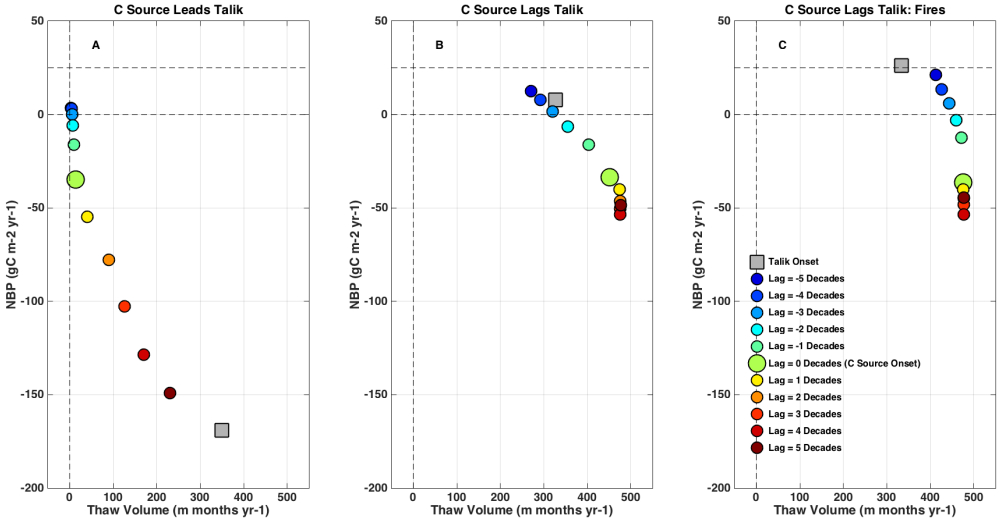

Figure 8. Net biome production (NBP) as a function of thaw volume. Symbols represent NBP and thaw volume values averaged over regions which transition to long term C source from 2060-2140, binned into regions where the decade of C source transition (A) leads talik onset, (B) lags talik onset, and (C) lags talik onset AND where fires exceed 25 g C m^{-2} yr^{-1}. Colors indicate decade relative to C Source transition, denoted by the large green marker, which occurs when NBP exceeds 25 g C m^{-2} yr^{-1} (grey horizontal dashed line). The grey square marker indicates the mean NBP and thaw volume values during talik onset. Cases where C source leads talik (A) show small thaw volumes during C source transition, and amplified C sources during talik onset. Cases where C source lags talik (B-C) show large thaw volumes during C source transition, and C sinks during talik onset.

The Cryosphere Discuss., https://doi.org/10.5194/tc-2017-189
Manuscript under review for journal The Cryosphere
Discussion started: 18 September 2017

914

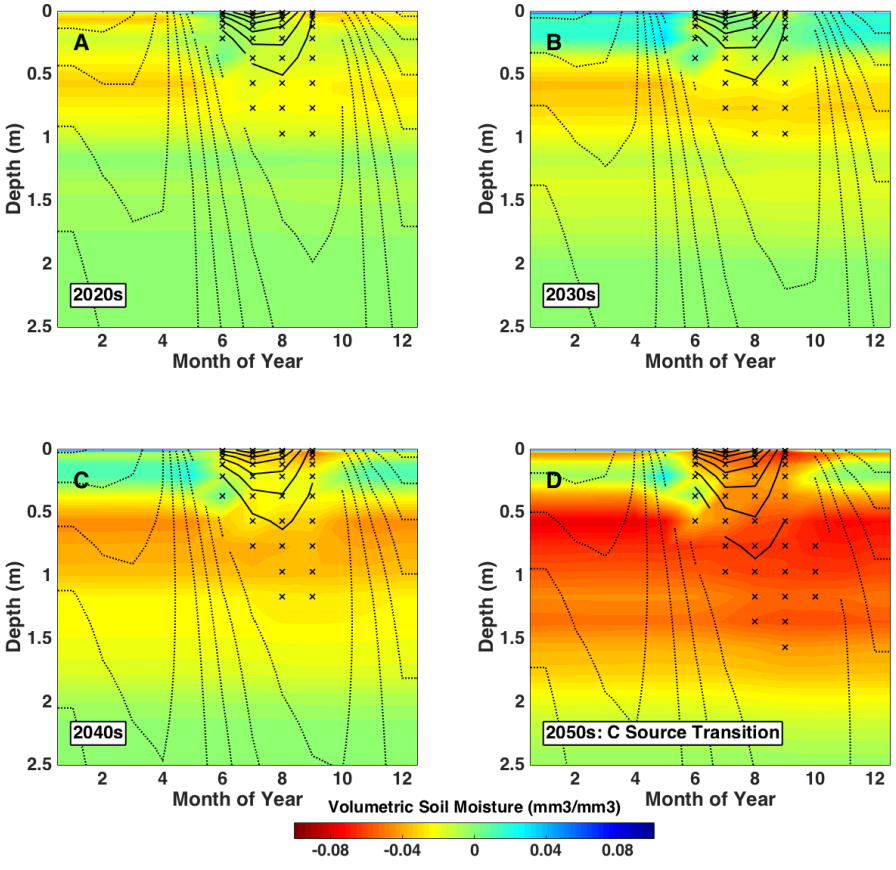

915

916 **Figure 9**. Evolution of simulated soil thermal and hydrological state, plotted as a function of
917 month and depth, for regions which transition to long term C sources in the 2060s but don't
918 form talik for another 3 decades (≥ 2090s). This represents cases where C Source leads talik
919 (e.g., Fig. 8B). Each panel presents decadal average seasonal profiles in the decades leading up
920 to C source transition. Shading and contour details are explained in Fig. 3. These profiles exhibit
921 shifts in thaw period (Oct), depth (> 1.5 m), and soil moisture (drying) in the transition decade.

922

The Cryosphere Discuss., https://doi.org/10.5194/tc-2017-189
Manuscript under review for journal The Cryosphere
Discussion started: 18 September 2017

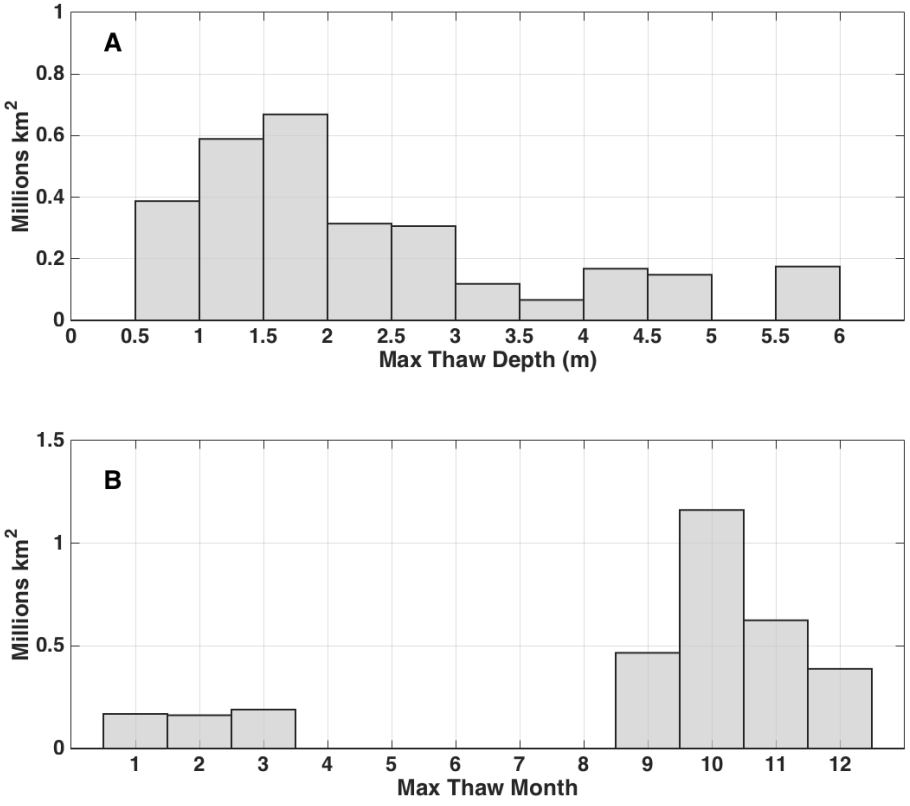

923

924 **Figure 10**. Histogram of total permafrost area as a function of (A) maximum thaw depth and (B)
925 maximum thaw month, for regions which transition to long term C sources prior to talik onset.
926 Here, thaw depth represents the depth of the active layer. This shows that most regions
927 transition to C sources when the active layer grows to a depth of 1-2 meters and reaches a peak
928 thaw month at depth (> 1 m) of October.

929

The Cryosphere Discuss., https://doi.org/10.5194/tc-2017-189
Manuscript under review for journal The Cryosphere
Discussion started: 18 September 2017

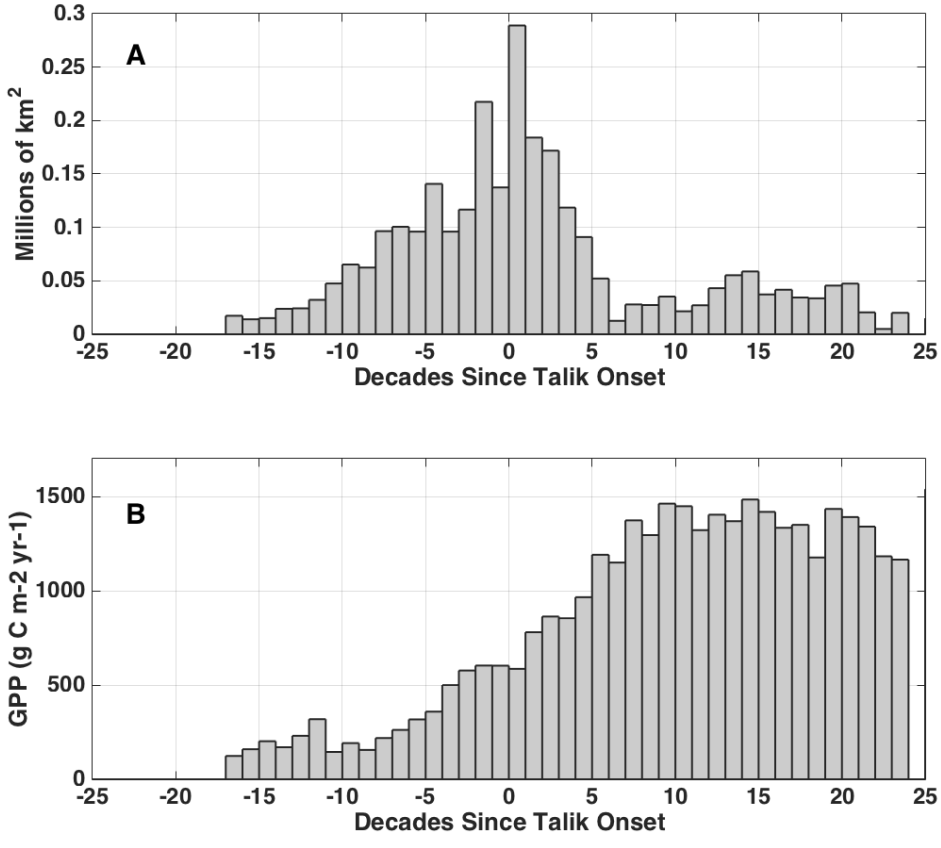

930

931 **Figure 11**. Histogram of total permafrost area (A) and mean GPP (B) as a function of decades
932 since talik onset. Regions with high initial soil organic matter (SOM > 100 kg m^{-2}) and fire C
933 emissions (Fire > 25 g C m^{-2} yr^{-1}) during the C source transition decade are removed, such that
934 factors driving the trimodal distribution when all regions are excluded (Fig. 7D). In the absence
935 of these factors, most regions transition to long term C sources in 1 decade following talik
936 onset. The large standard deviation (8 decades) is related to gross primary production (GPP),
937 with long transition periods (right tail) correlated to high productivity (GPP > 1000 g C m^{-2} yr^{-1})
938 and negative transition (C source onset in the absence of talik) correlated to low productivity
939 (GPP < 250 g C m^{-2} yr^{-1})

940

The Cryosphere Discuss., https://doi.org/10.5194/tc-2017-189
Manuscript under review for journal The Cryosphere
Discussion started: 18 September 2017

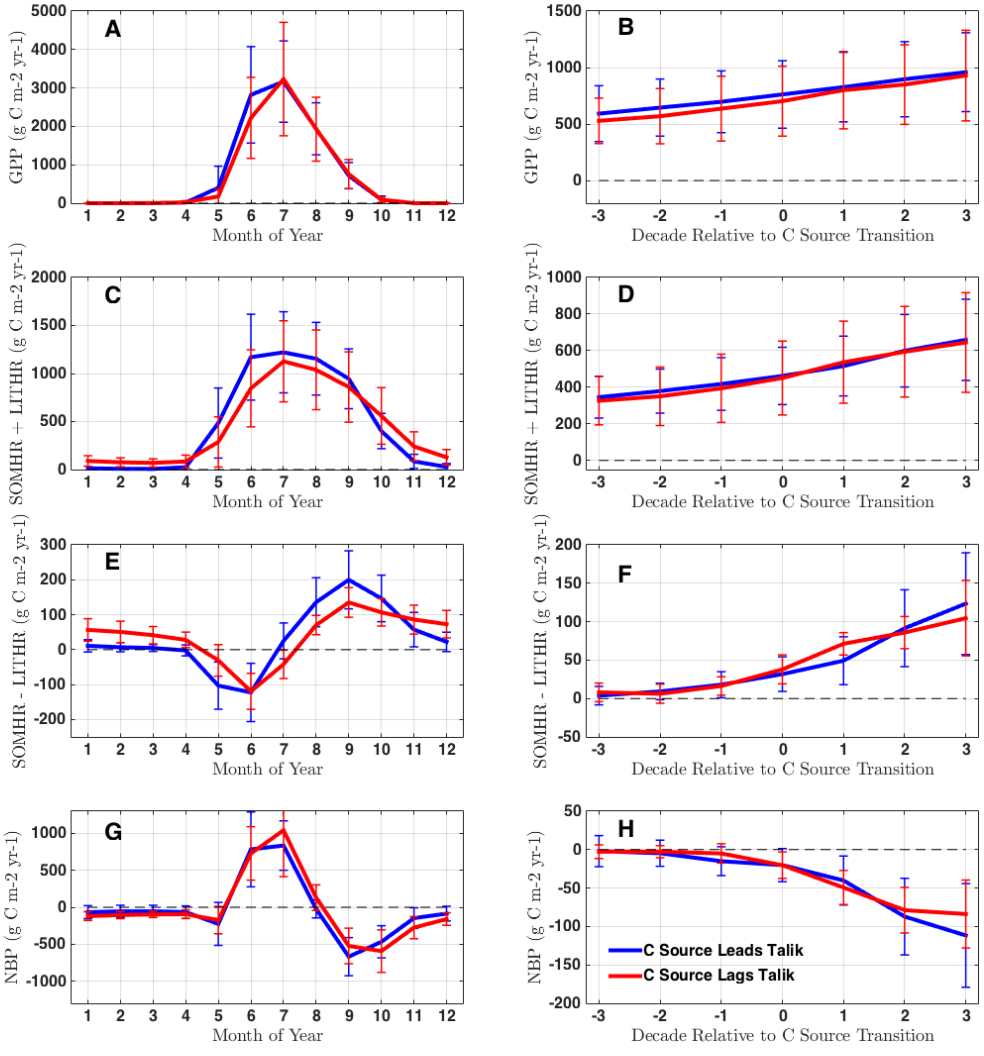

Figure 12. Time series of ecosystem C fluxes showing seasonal and decadal patterns during C source transition. This present results for (A-B) Gross Primary Production (GPP), (C-D) Sum of respiration from soils (SOMHR) and litter (LITHR), (E-F) Difference of respiration from soils and litter, and (G-H) Net Biome Production (NBP). The left column show seasonal fluxes during the decade of C source transition. The right column shows the evolution of decadal mean fluxes in the 3 decades preceding and following C source transition. Regions where C source transition

949 leads talik (blue) show similar patterns to regions where transition lags talik (red). Specifically,
950 this shows a sudden jump in respiration (F) during C source transition in both cases, which
951 corresponds in time and magnitude to the jump in NBP (H). The primary difference between
952 regions is the seasonal distribution of SOMHR vs LITHR (E), which shows a large soil respiration
953 source throughout the cold season in cases where C sources lag talik. This indicates an annual
954 source of deep old C.

955

956